Design, Model, and Control of a Low-Cost 3 Degree of Freedom Balancing Laminate Leg with an Actively Controlled Ankle Using Fundamental Controls Concepts

by

Taha Shafa

A Thesis Presented in Partial Fulfillment
of the Requirement for the Degree
Master of Science

Approved April 2020 by the
Graduate Supervisory Committee:

Daniel Aukes, Chair
Wenlong Zhang
Bradley Rogers

ARIZONA STATE UNIVERSITY

May 2020

ABSTRACT

This thesis introduces a new robotic leg design with three degrees of freedom that can be adapted for both bipedal and quadrupedal locomotive systems, and serves as a blueprint for designers attempting to create low cost robot legs capable of balancing and walking. Currently, bipedal leg designs are mostly rigid and have not strongly taken into account the advantages/disadvantages of using an active ankle, as opposed to a passive ankle, for balancing. This design uses low-cost compliant materials, but the materials used are thick enough to mimic rigid properties under low stresses, so this paper will treat the links as rigid materials. A new leg design has been created that contains three degrees of freedom that can be adapted to contain either a passive ankle using springs, or an actively controlled ankle using an additional actuator. This thesis largely aims to focus on the ankle and foot design of the robot and the torque and speed requirements of the design for motor selection. The dynamics of the system, including height, foot width, weight, and resistances will be analyzed to determine how to improve design performance. Model-based control techniques will be used to control the angle of the leg for balancing. In doing so, it will also be shown that it is possible to implement model-based control techniques on robots made of laminate materials.

TABLE OF CONTENTS

CHAPTER Page

LIST OF TABLES

Table Page

LIST OF FIGURES

Chapter 1

INTRODUCTION

It is commonly known among roboticists that animals have a unique ability to traverse various terrain with relative ease, especially in comparison to traditional wheeled mechatronic designs. This drives roboticists to develop bio-inspired locomotive robots to replicate this unique ability for more advanced mechatronic designs, however there are many barriers that stand in the way of these designs being practical. This research focuses on the design of a low-cost laminate leg and performs analysis to verify what the optimal design for the leg, with a particular emphasis on the foot and ankle, would be for walking and balancing capabilities.

This new leg design is composed of low-cost, compliant laminate material that preserves kinematic capabilities of existing designs while adding a third degree of freedom with an actuator for ankle rotation, resulting in a fully actuated system with three motors located at the suspended base of the leg. The ankle motor connects to the foot using a parallelogram link design that results in a 1:1 turning ratio between the motor and the ankle. In addition, located at the suspended base is an IMU, installed primarily for pitch measurements used as feedback data for balancing using an active ankle. To isolate the role the ankle plays in balancing for this new leg design, the leg will be modeled as an inverted pendulum of variable, mass-less length with a focused mass located at its tip, representing the weight of all three motors in the suspended base located at the robot's center of mass. The pendulum length will vary as the height of the robot changes due to the position of the two remaining motors. Through analysis, we will demonstrate dynamic behaviors achieved by the leg, show its ability to control leg forces, and analyze the advantages of adding a third

degree of freedom for ankle rotation.

This paper utilizes fundamental mechanical design and controls concepts to determine a design blueprint for a low-cost robotic leg. There are three major factors to take into account when selecting motors and building a leg: whether the motors will provide enough torque, whether they will be able to rotate fast enough to stabilize the system, and whether the system can support their weight. Often times, meeting one criterion means sacrificing another, and it becomes difficult to determine a design that accommodates all the needs of the system. All three criteria will be analyzed in detail; analysis using theoretical concepts will show what the advantages and disadvantages are to various foot sizes and ankle designs, and these will both be tied to the height and weight of the robot, and the material chosen for supporting leg links.

Chapter 2 of this paper will give a comprehensive introduction into previous work done developing leg designs and what the advantages and disadvantages of previous designs were. The challenges of robot locomotion will be highlighted, followed by methods that have been previously incorporated to solve the problem, and how those methods relate to design decisions discussed throughout this paper.

Chapter 3 will delve into detail about the experimental design process, materials chosen, the rational behind design parameters, and the advantages of utilizing a 5-bar mechanism design. One of the primary advantages to laminate manufacturing is low-cost, high speed manufacturing methods. Previous research [26] has shown that there are large deviations from theoretical analysis and the experimental performance of laminate robots, so initially the research was primarily experimental. Later developments have shown that purely experimental methods did not suffice in developing a feasible laminate leg design, so fundamental controls concepts and simulations were used to help determine next steps in designing the robot leg.

Chapter 4 goes into detail about the leg kinematics, how it achieves three de-

grees of freedom, and how the general design of the leg is supported by proceeding sections discussing torque requirements, speed requirements, and general stability requirements of the system. Simulations are shown in this section that show the experimental design's movement capabilities.

Chapter 5 discusses the inverted pendulum with torsional spring model used to analyze the ankle and foot of the system. This chapter also goes into some minor modeling work that is potentially helpful for future applications, but did not provide a lot of insight for design. The rationale behind the inverted pendulum model will be revealed, and it will be compared another model derived from using Kane's method to arrive at the system's dynamics given a simple 5 bar mechanism design structure. Both the model of the inverted pendulum and stability conditions will be discussed in detail as well. There will also be a brief discussion about how the motors tasked with lifting the foot can be thought of as underactuated double pendulums. These analyses can then be applied to design parameters regarding leg height, motor selection, and passive and active controllers for balancing.

Chapter 6 will give an overview of the torque requirements for the system. Torque requirements are important for the stabilization of the system; if the motors do not meet torque requirements, the motors will not be able to control the leg movement fluidly. This implies any attempt to balance the robot will fail because the torque required to stabilize the system will exceed motor limits, so the system will not move appropriately regardless of input commands. The section will not go into detail about the nonlinearities of the system that affect torque requirements because gathering enough data to determine those nonlinearities is considered future work for this project. This section will also discuss how torque requirements affect the maximum speed; implications of speed capabilities are discussed in further details in Chapter 7.

Chapter 7 discusses the speed requirements. By using simulations in MATLAB,

the system model can be utilized to determine the speed requirements for a stabilizing ankle as a function of leg height. Different controller performances are then compared and used with varying model parameters to help determine optimal ankle designs. Lastly, Chapter 7 delves draws conclusions based on all the simulations, calculations, and experimental work. In chapter 8, conclusions will be drawn regarding motors and how leg lengths affect torque and speed requirements, and what can be learned from simulations run on the ankle. Future work will also be discussed.

Chapter 2

BACKGROUND

2.0.1 Legged Robots

Previous work in bio-inspired robotics started with fully actuated systems. For humanoid robots that meant using ZMP (zero moment point) [13] tracking to create walking gaits for designs such as the Asimo [5] and Hubo [4]. Eventually, the desire to save energy, cost, and improve performance lead to designs of robots that utilized dynamics and controllers resulting in underactuated behavior (examples include Mable[2], Atrias[12], Cassie[18], Atlas[3]), where the degrees of freedom exceeds the number of actuators in the system. With these models, researchers have been able to develop robotic systems capable of walking on various terrain while avoiding obstacles [6]. Underactuated behavior was drawn from earlier work from hopping monopods [21], powered dynamic walkers, and passive dynamic walkers, where spring-like legs and compliance were first experimented with for analysis on the advantages of implementing such mechanisms.

Robot advancements were not unique to humanoid robots. Quadrupeds (BigDog[7], Minitaur[15], Doggo[14], MIT Cheetah 2[9] and Super Mini Cheetah[17]) and other robots, such as monopods [8], have been used to study both optimal design and gaits for walking, running, and jumping. Most notably is the incorporation of four bar linkage mechanisms, which again utilize compliance concepts, where the four bar linkage acts as a spring to help mitigate system energy use and manipulate each leg for various gait trajectories.

By studying animals, their gait trajectories for different types of locomotion, and

how they compare between each species [1], researchers have found a practical way to model robot locomotion is by using a spring-loaded inverted pendulum (SLIP) model [10] to replicate these gaits. By developing more efficient designs, researchers now have the ability to study new methods of developing optimal locomotive gaits through simulation [11], [16], [19] and experimentally [18], [20] utilizing deep learning techniques and controls that can deliver more promising results than traditional ZMP tracking techniques. The robotics community, however, has yet to develop a flexible, laminate leg, that can implement lessons learned from the previous research to develop cheaper designs that can take advantage of less rigid, flexible, spring-like links through knowledge gained from experimenting with SLIP locomotion models.

2.0.2 Laminate Robots

Laminate robots have been growing in popularity due to easy manufacturing techniques that take advantage of compliance in materials like cardboard, carbon fiber, and fiber glass, which can result in variable system stiffness. Currently, laminate robots (examples include HAMR[23], DASH[24], DynaROACH[25]) primarily take advantage of laminate materials for their low-cost and ease of manufacturing, but less so for compliance. Ongoing research aims to implement the compliance of soft, laminate material to expose whether varying system stiffness can prove advantageous in robot designs. This research aims to delve into how low-cost materials can be implemented in a general 3 degree of freedom leg design for bipeds and quadrupeds. Future work will go more in depth on how the compliant nature of flexible materials can be used as an advantage when it comes to bio-inspired robotics.

2.0.3 Modeling and Optimization

Traditional methods of modeling robots often utilize simplified dynamic models, such as the spring-loaded inverted pendulum (SLIP) model [10]. The SLIP model is useful in allowing robotics researchers understand the dynamics of leg stability, the energy needed for various gaits, and the effect of changing various model parameters when designing a leg. By adjusting the spring stiffness, the trajectory of the suspended base mass can be altered, more accurately mimicking desired locomotive behavior. Physics engines have also been used, such as MuJoCo[22] and Pybullet[11], to help utilize reinforcement learning techniques and model based control for robot locomotion. Specifically, in the case of Pybullet, reinforcement learning techniques are shown to be effective in allowing the Minitaur[15] to maneuver using multiple gait trajectories.

Chapter 3

LEG DESIGN ITERATIONS

3.0.1 Initial Design

This bipedal leg design, inspired from the leg design of a road runner, went through a number of design iterations before arriving at its final structure.

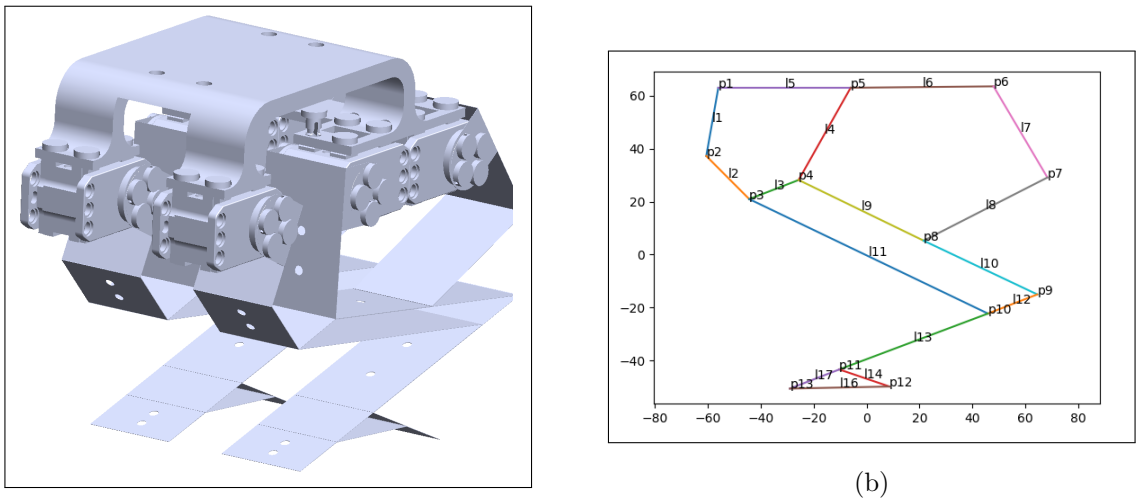

(a) (b)

Figure 3.1: 3D rendering (a) and kinematics (b) of V1 road runner inspired leg

The design rendering and kinematics can be viewed in figure 3.1. Since the goal was to create a fully actuated three degree of freedom system, three Dynamixel XL-320 servos were mounted to create legs that moved horizontally and vertically, along with an ankle that could rotate the body. The most pressing issue with this design was that the leg could not stand, but the reason was not certain. There were two theories, one was that the laminate material was not capable of holding up the motors, while the other was that the design needed to be improved, meaning it would not be

able to stand regardless of how rigid the leg links were. The immediate goal was to design a laminate leg that could balance itself and eventually be used for walking, so extensive redesign work was undertaken to arrive at a new leg structure.

3.0.2 Design - Version 2

Due to the quick and low-cost nature of laminate materials, the initial design stages were primarily experimental, with the exception of simulations in python to help guide the new design structure. Previous research regarding a hopping laminate robot[26] showed that there could be large deviations from simulated flexible dynamics to data gathered experimentally, so the conclusion was reached to attempt an experimental approach for the early stages of this project.

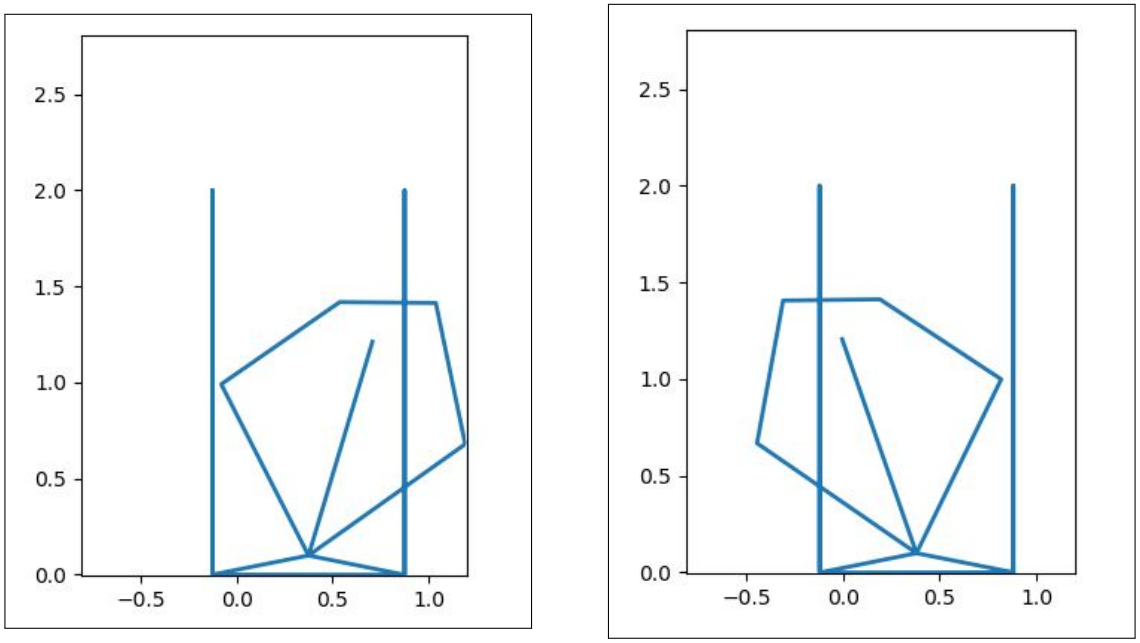

Figure 3.2: Stability of 5Bar Mechanism as Function of Foot Size

Initially, the goal was to create a three degree of system capable of holding its own

weight. The leg design was simplified to a 5 bar mechanism inspired by previous leg designs like UPenn's Mintaur and Stanford's Doggo. By simplifying the leg, it would be easier to isolate where the problem areas of the original design were, eventually with the goal of making the leg more complex to better mimic the original bio-inspired road runner model. Through physics simulations on python, it was concluded that for a standing leg, stability was determined primarily by whether or not the center of mass was located above the foot. Figure 3.2 shows a simulation where a 5 bar mechanism moves from one side to the next over the foot without falling. Figure3.3 shows a simulation where the same 5 bar mechanism moves to a location where its center of mass is no longer directly above the foot, and how that causes the leg to fall.

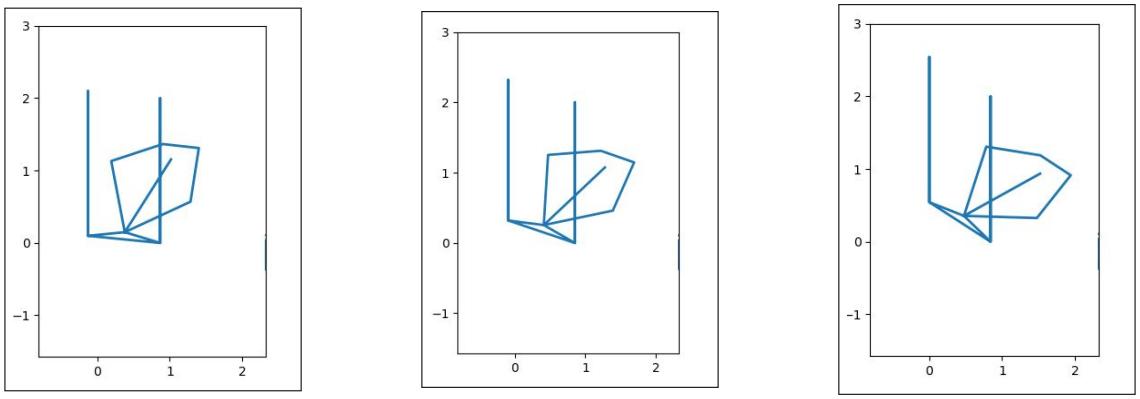

Figure 3.3: Unstable Position of 5Bar Mechanism as Function of Foot Size

Simulations and the success of previous designs (examples discussed in background section) motivated the next design to be a 5 bar mechanism with motors centered above the foot. The motor locations with the 3D suspended base holding them together can be viewed in Figure 3.4b and Figure 3.4a. Originally, to create this leg, 5 layered links of cardboard were used at a total thickness of 1.06 mm, however this

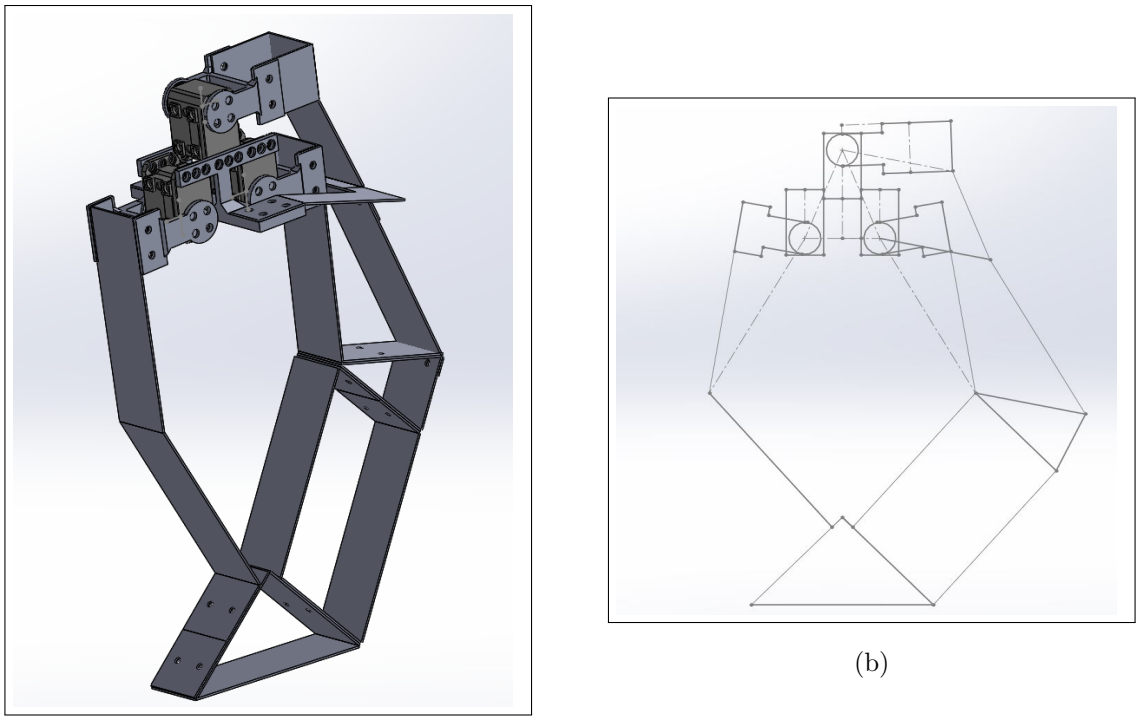

(a)

(b)

Figure 3.4: 3D rendering (a) and 2D rendering (b) of V2 biped

was not rigid enough to hold the weight of the three motors, so the leg still could not stand. The thicknesses of the links were then increased to 2.56 millimeters to increase the stiffness in the material, and the design that followed was able to stand (as shown in figure 3.5a). From both the 3D Solidworks rendering in Figure 3.4a and 2D geometric depiction in Figure 3.4b, it appears that this new design does a better job of centering the motors over the foot, but there were still issues remaining with the position of the leg's center of mass.

To control the ankle, there exists links around the outside of the leg tasked with rotating the ankle as the top actuator turns. Figure 3.4b illustrates how parallelograms were used to connect the top actuator to the foot for a 1:1 turning ratio from actuator to ankle. Although this model could stand, its center of mass was not cen-

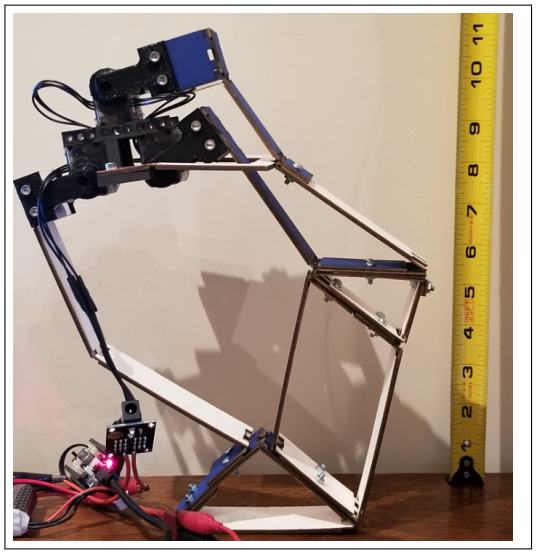

(a)

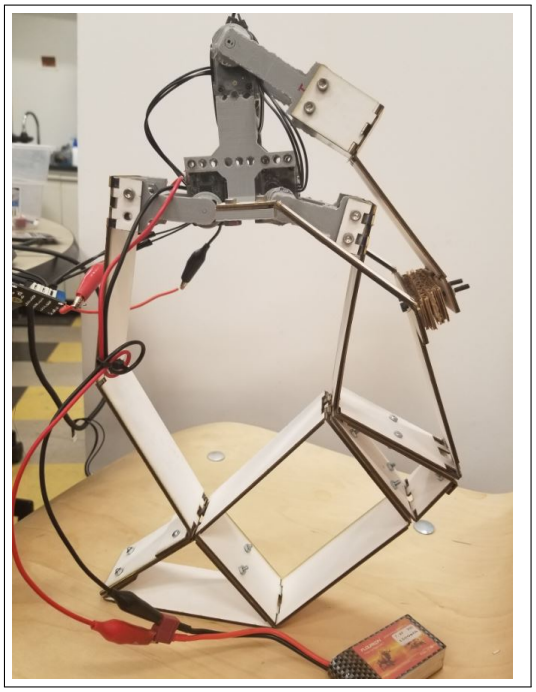

(b)

Figure 3.5: Standing Leg (a) V2 Altered Leg (b) of V2 biped leg

tered at the middle of all three motors as previously predicted. This was the case for two reasons. Since the laminate materials are light, their weight seemed negligible in comparison to the weight of each motor and the attached servo horns, so when taking the mass of the entire system, the links were considered massless, even though in reality they carried weight. The miscalculation of the system's center of mass brought on by this assumption was worsened because all Dynamixel XL-320 motors used in this design iteration were all relatively light as well, weighing about 16.7 grams each. In addition, the top servo horn faced one direction and leaned its weight heavily onto one side, so the combined weight of the links and 3D printed servo horn in tandem with each servo weighing so little resulted in a center of mass that was not directly above the foot.

Even though this new model could stand, there were a number of issues. First, the servo horns did not produce enough torque to fluidly maneuver the robot in any direction. This meant that an effort to control the leg to perform in any way beyond standing in place would be impossible because the motors did not have enough torque to move and stabilize the links. Also, figure 3.5b reveals a flaw in the constraints of our leg design. The servo horn directly below the top horn is incapable of its full range of motion because of unwanted contact between it and the ankle link. This is undesirable because it hinders the necessary range of rotation for each servo for this leg to eventually walk. Lastly, the center of mass needed to be moved directly above the foot to make future applications of the leg design more feasible.

3.0.3 Final Design - Version 3

To fix issues from the previous design iteration, a number of steps were taken when developing this new design. First, the motors were changed to Dynamixel 430-W350T models to fix torque issues from the previous design iteration. In addition, the leg design is now symmetric to keep the center of mass directly above the foot. Lastly, to keep any unwanted contact between links, the top links directly affecting ankle rotation have been changed. The new leg design can be viewed in figure 3.6 and a side by side comparison of the two motors used between iterations can be viewed in table 3.1.

Dynamixel Motor	No Load Speed	Stall Torque	Gear Ratio	Weight	Cost
XL320	114 RPM	0.39 N-m	238:1	16.7g	$21.90
XM430-W350-T	46 RPM	4.1 N-m	353.5:1	82g	$229.90

Table 3.1: Dynamixel XL-320 and XM430-W350-T Comparison

The current design is built with three motors, two controlling the oscillatory mo-

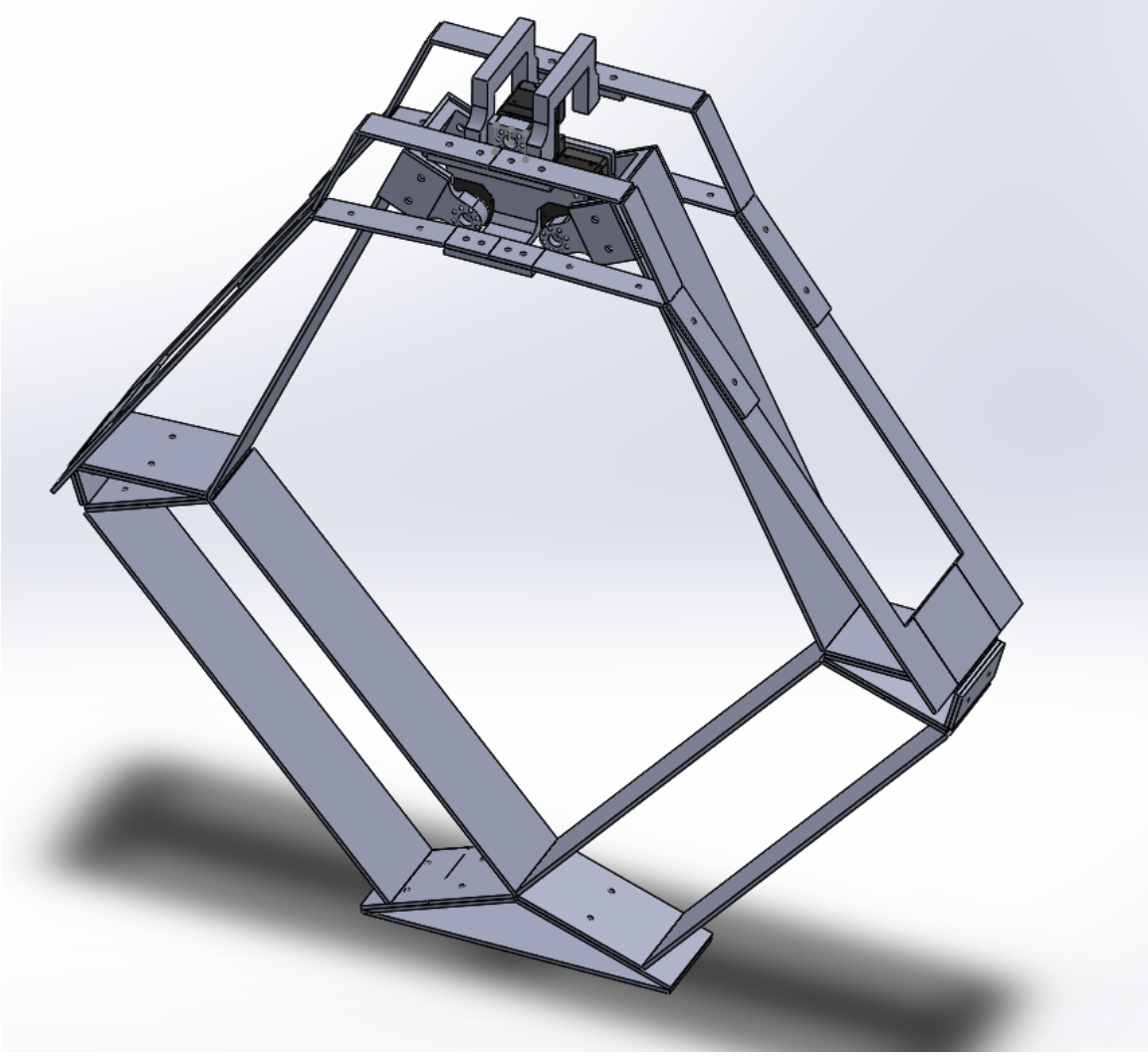

Figure 3.6: CAD Model of Robot Leg

tion of the leg, and one controlling ankle rotation. Since the leg links are made of cardboard, all links were assumed to be massless when doing calculations, as they contribute little weight in comparison to the combined weight of these three 82 gram motors. Each motor contains a stall torque of 4.1 newton meters, and a no load speed of 46 revolutions per minute. The system in total weighs about 629 grams, 256 grams from the motors, and the rest from the 3D printed parts and screws needed to assemble the leg. Each motor can rotate without any load at around 4.2 radians

per second. The joint limits introduced by the previous design iteration have also been improved, with each of the three motors being able to spin around 90 degrees, giving the robot leg a rich control space to operate. By completing this final experimental design iteration, the initial goal of developing a three degree of freedom leg design capable of standing and potentially balancing and walking has been completed. Through experimentation, an optimal laminate design has been reached for a three degree of freedom leg capable of standing and high level design performance. For the next step, analysis needs to be done to determine how varying the leg height affects the system, how varying foot size affects the system, and what specifications the actuators should have to develop robot legs optimal for various uses.

Chapter 4

KINEMATICS

The evolution of the leg kinematics for each leg design are critical in understanding how the system can move and whether the leg is capable of eventually balancing and walking. The goal of this section is to observe the evolution of kinematic capabilities of the system in an effort to better understand how the system moves.

Figure 4.1 displays the original 3 degree of freedom system and its three degree of freedom motion capabilities. The evolution of the bipedal design stemmed largely from this first design's inability to stand or balance itself. Inspired from the leg structure of a roadrunner, this design utilized three motors in a fully actuated system for three degrees of freedom, using two motors to provide oscillatory behavior to the top links that would manipulate the foot's location in a two dimensional plane. A third motor was then installed to twist the ankle. Although the leg could not stand,

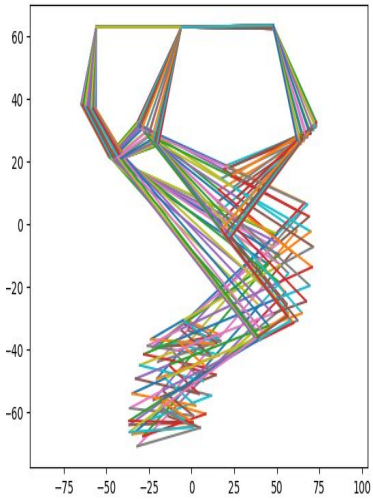

Figure 4.1: Kinematics of Original Design

the same general idea was implemented in future designs, where two motors were utilized to move the position of the foot in a two dimensional plane, while the third motor controlled the rotation of the ankle for balancing.

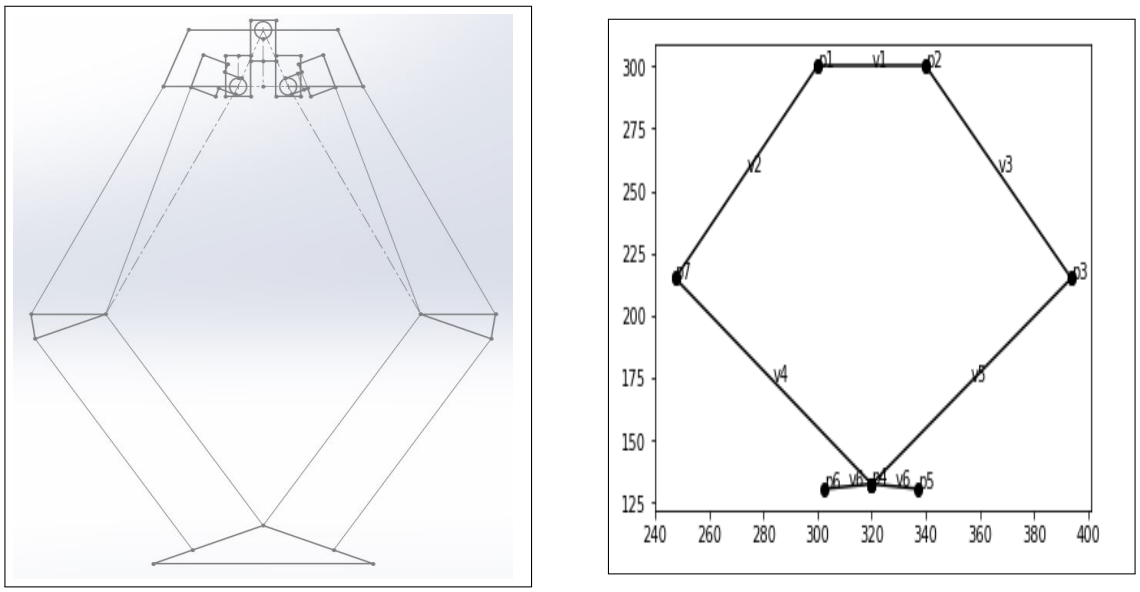

(a) (b)

Figure 4.2: Two Dimensional Rendering of Final Experimental Design (a) and Python simulation 5 Bar Mechanism (b)

As the designs developed, a need to keep all three degrees of freedom drove us to create simulations in python to determine the properties of motion of the system. A two dimensional rendering of the final design can be viewed in Figure 4.2a, which shows clearly that all three motors are located at the suspended base, where the bottom two are connected to the traditional 5 bar linkage, while the top motor is connected via parallelograms to the foot. Figure 4.2b represents how the design can be simplified for the python simulation while maintaining the same basic design structure and what each link and vertex is labeled as. This design was chosen because it centers the center of mass over the foot, which shown previously allows the leg

to stay upright, and it retained its three degrees of freedom. To test whether the three degree of freedom movement capability of the robot leg was preserved for the final design, the kinematics were simulated for a 5 bar linkage design, similar to the simulation run to determine the kinematic capabilities shown in Figure 4.1.

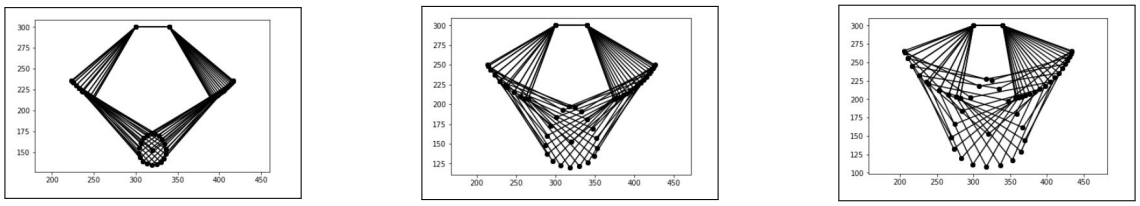

(a) (b) (c)

Figure 4.3: Kinematics of 5 Bar Linkage with Amplitude of 10 (a) 20 (b) and 30 (c)

$$\theta_{i1} = A_{i1} * \sin(\omega_i t - \phi_{i1}) + o_{i1} \tag{4.1}$$

$$\theta_{i2} = A_{i2} * \sin(\omega_i t - \phi_{i2}) + o_{i2}, \tag{4.2}$$

The images in Figure 4.3 display the planar movement capabilities due to the two bottom motors (shown in Figure 4.2b as p1 and p2) in the final design by applying a sinusoidal input into a python simulation and tracking the position of the leg's end effector. The sinusoidal inputs are shown in Equations 4.1 and 4.2, where i indicates a motor number, A_{i1} and A_{i2} indicate the amplitude of each servo, ω_i is the (coupled) frequency of the two actuators, ϕ_{i1} and ϕ_{i2} are the time offsets in the sine function, and o_{i1} and o_{i2} are offsets that correctly align the output of the motors with the corresponding positions of their connected links. Figure 4.3 shows the ability for a 5 bar mechanism to manipulate its end effector at increasing amplitudes to illustrate the large control space offered by the design, which will be required when transitioning from balancing to walking.

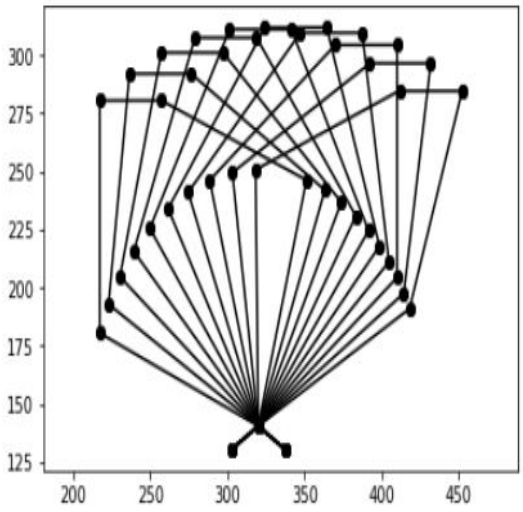

Figure 4.4: Kinematics of Ankle for 5 Bar Mechanism with Parallelogram Structure from Motor to Foot

Through simulation, it could be shown that a 5 bar linkage has the capability of supplying two degrees of freedom to the robot leg system with more control space than the original design. By observing Figure 4.2b, one can note that the 5 bar mechanism is essentially two double inverted pendulums tied together with a fifth bar at the top. This becomes important when modeling the system and determining the torque requirements for the suspended base to lift the leg. It is equally important to design a robot that can both balance and walk, so when designing the leg, it is important to determine not only how well the biped can stabilize itself, but whether or not the motors have enough torque to lift the leg when walking. More detail will go into the modeling of a double pendulum in Chapter 5 and how that model relates to the torque requirements in Chapter 6.

The next step was to determine a way to create a third degree of freedom at the ankle. Difficulties arose when determining the best way to control the ankle. The leg needs to not only be controllable, but as easy to control as possible if this low-cost

design were to eventually make it into multiple labs and classrooms. In addition, traditional ankle motors are located at the ankle of the robot (examples include HUBO and Asimo), however this is impossible due to the material used to design the leg. Cardboard links would have a hard time lifting the weight of the ankle motor, and in addition to the links potentially breaking, this would require additional torque requirements on the two oscillating motors manipulating the 5 bar linkage, creating an infeasible design. Instead, the third motor is placed at the top of the robot, as seen in Figure 4.2a, and is connected to the foot using parallelogram structures that created a 1:1 turning ratio between the top motor and the twisting motion of the foot.

Since the parallelograms connecting the ankle actuator to the foot created a 1:1 turning ratio between the actuator and foot, the simulation shown in Figure 4.4 could accurately mirror the movement created by the ankle actuator by rotating the suspended base of the 5 bar mechanism about p4. Python simulations shown in Figures 4.3 and 4.4 show this 5 bar mechanism inspired design will not only have three degrees of freedom, but it will have a larger movement space than its predecessor design.

This solver is fairly effective at modeling the movement of the leg and will fail when the device moves through a singularity, if the step size between actuator positions grow too large, or if the inputs to the system (inputs to p1, p2, and p4) are too large so that they force the leg to move away from a valid solution. Only by doing an analysis of the kinematics of our final design were we able to verify that the 5 bar mechanism with parallelogram links connecting the ankle actuator to the foot would fit all the preliminary design requirements of the system and result in a leg that could stand.

Chapter 5

MODEL OF 5 BAR MECHANISM WITH CONTROLLABLE ANKLE

5.0.1 Pynamics Model

When modeling the system, the first inclination was to derive a model of the 5 bar mechanism with three controllable actuators reading back both position and velocity. The model could be derived by hand, then linearizing the system over a certain equilibrium point, and arriving at the A, B, C, and D matrices. Instead, a program titled pynamics was utilized. It is a python simulation tool that uses scipy's odeint function, sympy to represent equations and apply derivatives, and Kane's method to derive equations of motion.

$$\begin{bmatrix} \dot{\theta}_1 \\ \ddot{\theta}_1 \\ \dot{\theta}_2 \\ \ddot{\theta}_2 \\ \dot{\theta}_3 \\ \ddot{\theta}_3 \\ \dot{\theta}_4 \\ \ddot{\theta}_4 \\ \dot{\theta}_5 \\ \ddot{\theta}_5 \end{bmatrix} = \begin{bmatrix} 0 & 1 & 0 & 0 & 0 & 0 & 0 & 0 & 0 & 0 \\ 192 & -0.8 & 715 & 0.4 & 0 & 0 & 0 & 0 & 0 & 0 \\ 0 & 0 & 0 & 1 & 0 & 0 & 0 & 0 & 0 & 0 \\ -365 & 0.4 & -132 & -0.4 & 0 & 0 & 40 & 0 & 0 & 0 \\ 0 & 0 & 0 & 0 & 0 & 1 & 0 & 0 & 0 & 0 \\ 0 & 0 & 0 & 0 & -80.3 & -0.8 & 40 & 0.4 & 0 & 0 \\ 0 & 0 & 0 & 0 & 0 & 0 & 0 & 1 & 0 & 0 \\ 0 & 0 & 40 & 0 & 40 & 0.4 & -80 & -0.4 & 0 & 0 \\ 0 & 0 & 0 & 0 & 0 & 0 & 0 & 0 & 0 & 1 \\ 1.23 & 0 & 4.34 & 0 & 0 & 0 & 0 & 0 & -40 & -4 \end{bmatrix} * \begin{bmatrix} \theta_1 \\ \dot{\theta}_1 \\ \theta_2 \\ \dot{\theta}_2 \\ \theta_3 \\ \dot{\theta}_3 \\ \theta_4 \\ \dot{\theta}_4 \\ \theta_5 \\ \dot{\theta}_5 \end{bmatrix} + \begin{bmatrix} 0 \\ 1 \\ 0 \\ 1 \\ 0 \\ 0 \\ 0 \\ 0 \\ 0 \\ 1 \end{bmatrix} \tau \tag{5.1}$$

Equation 5.1 displays the state space model of the A and B matrices for the model

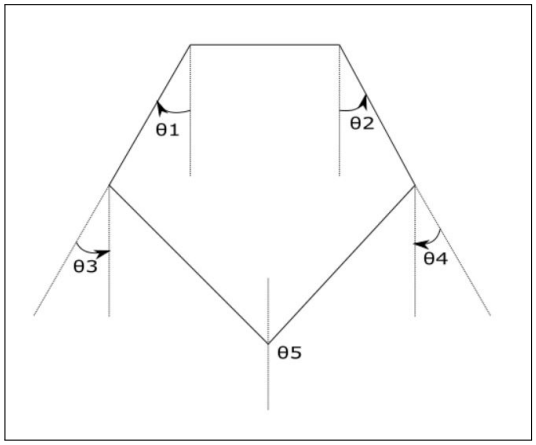

(a)

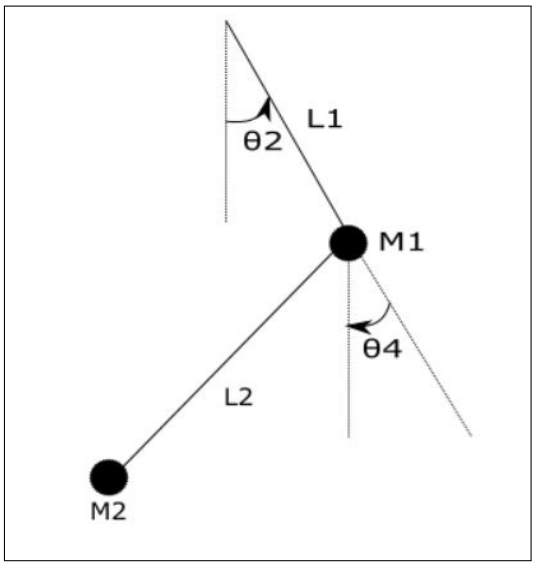

(b)

Figure 5.1: Diagram of States for Pynamics Model (a) and double pendulum (b)

linearized about $\theta_1 = 30$, $\theta_2 = 30$, $\theta_3 = 90$, $\theta_4 = 90$, $\theta_5 = 0$ and every $\dot{\theta}$ term equal to 0 (system at rest). There are some issues using python to arrive at the state space model using pynamics. When attempting to model a system, it is not always wise to arrive at the model without attempting to simplify it first. Little is known about the system and how the assumptions made would negatively effect performance. Models are never perfect to begin with, so if the model is complex, such as the case with this tenth order system, it will be difficult to isolate where the issue is arising from. For example, when arriving at this model, rigid body dynamics were assumed, even though there is compliance in the material. It would be difficult to tell if the system's controller did not work if that was a problem with the controller or the model. Even if a controller is built for the robot leg, and the simulations run for the controller are promising, if those simulations fail when applied experimentally, with a complex model, it will be difficult to isolate why the model failed. It could lead to a situation

where an engineer invests a large amount of time that largely goes wasted because there is no way to easily isolate why the system is not working. Instead, it was more desirable to arrive at a simpler model for balancing, and then potentially to use this pynamics model or a model like it for more complicated higher level control needs.

Also, the design may have developed experimentally, but there are still issues to address when it comes to the design of the system. Although the motors selected meet torque requirements, it is not clear whether or not it can balance or walk, so the most important contribution controls concepts can provide at the moment is not higher level controls, but insight on preferable design parameters, and the complex tenth order system in Equation 5.1 does not offer very much design insight, but the double pendulum and the simplified inverted pendulum do.

5.0.2 Double Pendulum

Figure 5.1b illustrates how one side of 5 bar linkage can be expressed as a double pendulum, thereby making the entire 5 bar mechanism two double pendulums connected together at the base and at the top by a fifth bar. The force, or torque, each motor must exert to lift the foot, can be expressed as $\ddot{\theta_1}$ and $\ddot{\theta_2}$, with locations consistent with the locations of θ_1 and θ_2 in Figure 5.1a. The model of a double pendulum is expressed in Equation 5.2, which goes off the labels in Figure 5.1b.

$$\ddot{\theta_2} = \frac{-g(2m_1 + m_2)sin(\theta_2) - m_2 g sin(\theta_2 - 2\theta_4) - 2sin(\theta_2 - \theta_4)m_2(\dot{\theta_4^2}L_2 + \dot{\theta_2^2}L_1 cos(\theta_2 - \theta_4))}{L_1(2m_1 + m_2 - m_2 cos(2\theta_2 - 2\theta_4))} \tag{5.2}$$

Equation 5.2 solves for the angular acceleration corresponding to one of the two motors that allows for the two degree of freedom planar motion of the foot. Although for the purposes of early design and motor selection, Equation 5.2 does not help much with torque calculations, it does give insight into how the system works, and

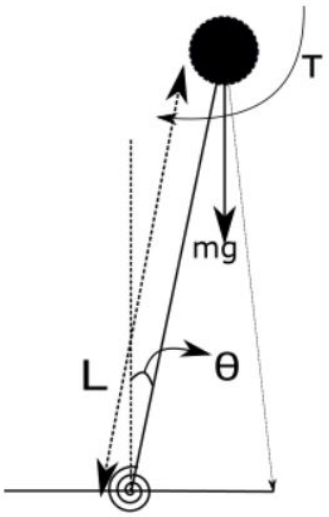

Figure 5.2: Diagram of Inverted Pendulum with Labeled States, Forces, and Parameters

it is important to understand the model moving forward to provide more insight into the dynamics of the system.

5.0.3 Inverted Pendulum Model

The design of the ankle has a motor actively controlling its position, however, it is unclear whether or not the best ankle design is one actively controlled by a motor, or a passive ankle controlled by a spring. To determine what the optimal design may be for legs of varying heights, it makes most sense to model the robot leg as an inverted pendulum. Doing so will isolate the effect the ankle has on the system, which has the most effect on balancing the system when both legs of the biped have contact with the ground. From there, analysis of the system behavior under disturbances will determine the advantages or disadvantages of particular ankle designs. A diagram of the inverted pendulum with applied torque is shown on Figure 5.2. For the simplicity of analysis, we initially assume no damping.

Equation 5.3 displays the ordinary differential equation for an inverted pendulum model with an active ankle and torsional spring.

$$ml\ddot{\theta} = \tau - k\theta - b\dot{\theta} + mglsin(\theta) \tag{5.3}$$

The matrices shown below in equation 5.4 show the state space model linearized around $\theta = 0,\ = 0, \mu = 0$

$$\begin{bmatrix} \dot{\theta} \\ \ddot{\theta} \end{bmatrix} = \begin{bmatrix} 0 & 1 \\ \frac{-k}{ml^2} + \frac{g}{l} & \frac{-b}{ml^2} \end{bmatrix} + \begin{bmatrix} 0 \\ \frac{T_{max}}{ml^2} \end{bmatrix} \tag{5.4}$$

Equations 5.3 and 5.4 can be utilized to arrive at the system's transfer function in terms of the pendulum's angular position as the output. The transfer function is shown in equation 5.5

$$\frac{\theta(s)}{\tau(s)} = \frac{\frac{T_{max}}{ml^2}}{s^2 + \frac{bs}{ml^2} + \frac{k}{ml^2} - \frac{g}{l}} \tag{5.5}$$

For a completely active ankle, when assuming the damping coefficient and torsional resistance to be 0 for the simplicity of analysis, we are left with with a system with two poles, one stable, and one unstable, both located equidistant from the origin at a distance of $\sqrt{\frac{g}{l}}$ as seen in Figure 5.3.

The transfer function shown in equation 5.5 can also be used to determine the k values needed for the torsional resistance to stabilize the system. A system's stability relies solely on the location of its poles, which can be found in the system's characteristic equation shown in the denominator of equation 5.5. Notice that when setting the damping coefficient to be 0, the system is revealed to be marginally stable as long as the relation in equation 5.6 holds.

$$\frac{k}{ml^2} - \frac{g}{l} > 0 \tag{5.6}$$

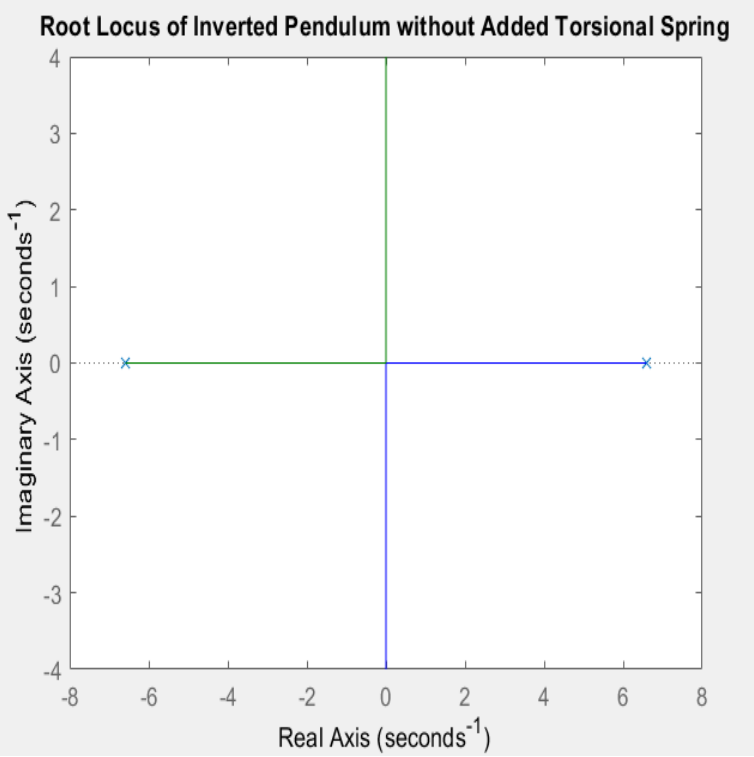

Figure 5.3: Placement of Poles for Robot Leg

It is important to note that although this condition results in marginal stability theoretically, all systems have some damping, which drags these marginally stable poles into the left half plane, resulting in a stable system exhibiting decaying oscillatory behavior.

Note that there cannot be enough damping to drag the right half plane zero to the left half plane when the stability condition in equation 5.6 is not met. If enough damping were introduced to the system to drag the poles in figure 5.3, the system would no longer be an inverted pendulum, it would be a pendulum locked in its unstable equilibrium point without the freedom to move. This means that for there to be a stable, balancing system, there would either need to be a spring at the ankle to act as a proportional controller, a motor with a high enough bandwidth to stabilize the system in the face of disturbances, or a motor and spring working together, where

the spring acts as a proportional controller to take care of high frequency disturbances, while the actuator helps stabilize lower frequency disturbances for improved performance.

Chapter 6

TORQUE REQUIREMENT ANALYSIS

As explained previously, the torque requirements for the two motors creating the two degree of freedom planar motion of the leg can be determined by the double pendulum model, while the torque requirements of the actuator controlling the ankle are best explained by the inverted pendulum model. The angular velocity relationship in Equation 5.2 corresponds to the torque needed for an actuator to lift the leg, while the angular velocity relationship in Equation 5.3 corresponds to the torque needed for an actuator to rotate the leg around the foot.

6.0.1 Double Pendulum

The primary goal for the early stages of system design is determining the optimal motors for motion and stabilization. To determine the torque requirements, we must

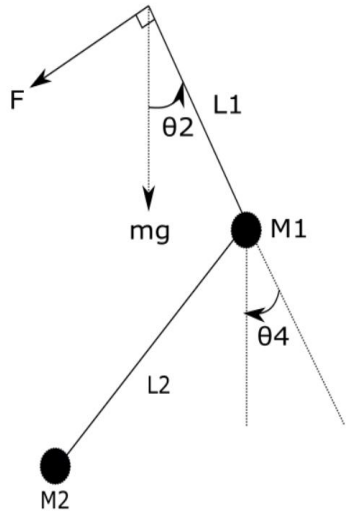

Figure 6.1: Diagram of Applied Torque onto Motor

determine the torque needed in the worst case orientation of the system; by choosing actuators that can provide enough torque to lift the robot in the worst case, we have designed a system that can manipulate suspended base and end effector for all cases. This motivates the next step, which is to determine the worst case. Take the general case for calculating torque shown in Equation 6.1, where τ is the torque, r is the radius, and F is the force perpendicular to the radius of the beam.

$$\tau = L_1 F_{mg} cos(90 - \theta_2) \tag{6.1}$$

$$F_{mg} = mg \tag{6.2}$$

The motor located at θ_2 exerts a force that pushes from the other side of the beam to lift the suspended base. According to the calculation in equation 6.1, the closer θ_2 is to 90 degrees, the more torque is required of the motor to turn, which makes sense, since τ is calculated by the force being exerted perpendicular to its moment arm. Typical measurements for θ_2 can be 45 degrees or greater, and calculating for τ at $\theta_2 = 45$, considering the mass of the system for standing design iteration with Dynamixel XL-320 motors to be about $400g$, and the length of the lever arm $L_2 = 0.2m$, the calculated $\tau = 0.41Nm$. This exceeds the stall torque of the first motors (rated at $0.39Nm$), and may explain why motors with larger torque were needed for the next design iteration.

6.0.2 Inverted Pendulum

The torque exerted by the active ankle can be calculated using Equations 6.3, 6.4, 6.5, and 6.6. Equation 6.3 shows the torque applied is proportional to the peak power over the speed in revolutions per minute (RPM). The term 9.549 is the conversion factor from RPM to radians per second needed to arrive at is applied $\tau_{applied}$ in newton

meters. The $\tau_{applied}$ found can be applied to the following equations until the total torque on the foot is finally calculated in Equation 6.6.

$$\tau_{applied} = \frac{9.549 * Power_{Watts}}{Speed_{RPM}} \tag{6.3}$$

$$\tau_{Foot} = rF \tag{6.4}$$

$$\tau_{mg} = mgLsin(\phi) \tag{6.5}$$

$$\tau = \tau_{Foot} - \tau_{mg} + k\theta \tag{6.6}$$

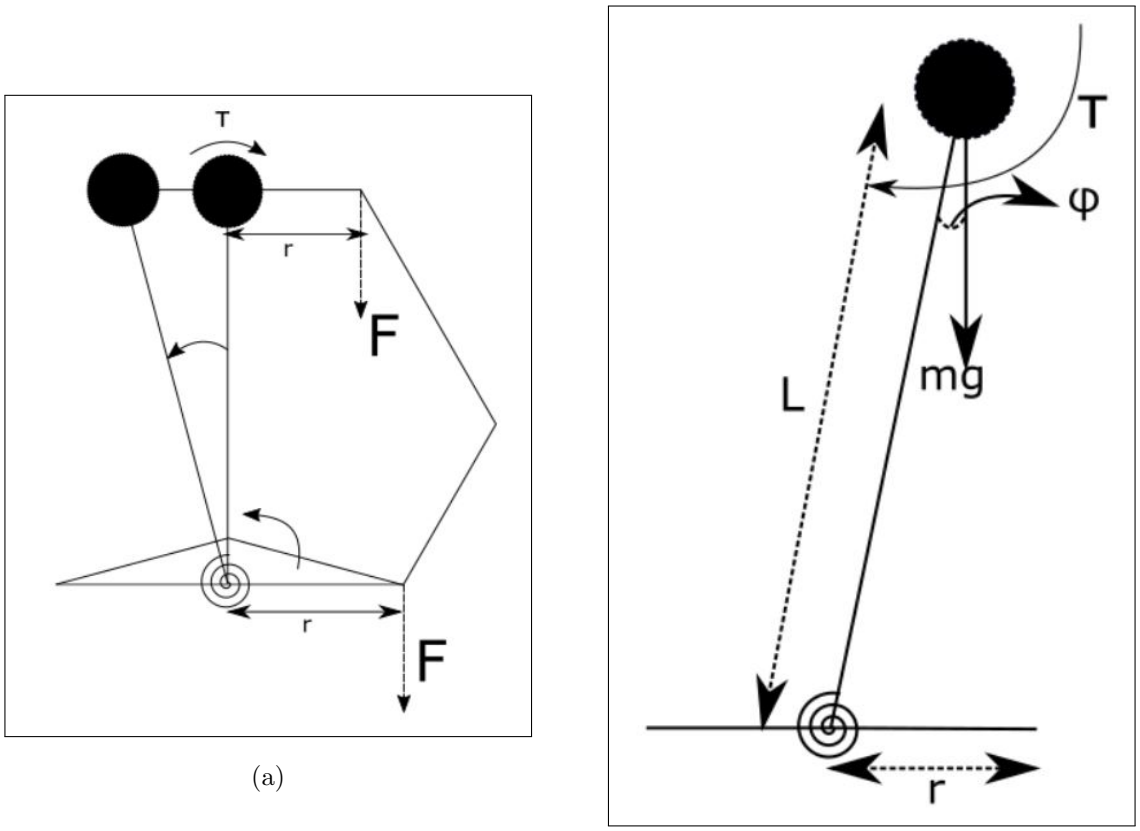

(a)

(b)

Figure 6.2: Diagrams of Inverted Pendulum with Applied Torque

Figures 6.2a and 6.2b illustrate the effect of torque on the inverted pendulum

model. Figure 6.2b shows how gravity adds to the torque, while figure 6.2a calculated how the torque from the actuator directly affects torque applied to the base of the inverted pendulum. To get an accurate measure of τ_{Foot} in Equation 6.4, the manufactured leg can be placed on a force sensor and by reading the force, one can determine what torque is needed to rotate the body. The total torque τ used to rotate the system is a function of the total height, the length of the foot, the mass of the system, and the speed at which the motor is spinning. These relations show that the taller the system, the larger torque is necessary to exert on the system. In other words, if the inverted pendulum is to be thought of as a lever arm, the longer the lever arm, the more torque is needed to move the inverted pendulum. In addition, Equation 6.5 reveals that longer lever arms add more torque in the opposite direction of the applied torque when stabilizing the system, ultimately decreasing the total torque exerted onto the ankle (shown in 6.6).

It is also important to note that the taller the system, the less rotational speed the robot will need to stabilize. This illustrates the fundamental trade off when selecting motors, that these designs must be tall enough to meet the bandwidth requirements for speed, but also that these motors need to generate enough torque to move the system fluidly. In addition, when considering the massless, flexible links being used to develop the robot leg, longer links contribute to more bending and spring-like behavior in the system, which could be either advantageous or detrimental depending on the desired spring stiffness of each link. However, for early design stages, compliance will not be taken into account, and all links will be assumed rigid due to the thickness of the laminate material.

Equation 6.4 and Figure 6.2a show that one way to reduce torque requirements from the motor is to increase the width of the foot; increasing the width of r increases the torque output for the active ankle (note that Figure 6.2a labels accurately that

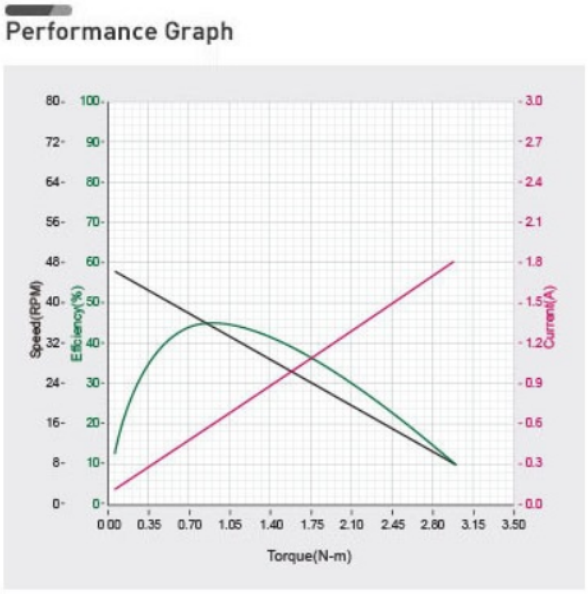

Figure 6.3: Performance Graph of selected XM430-W350-T motor

the width of the foot from the center of the robot is equal to the width of lever arm connecting the ankle actuator to the foot). Again, assuming massless links, this can only serve to improve the performance of the robot when balancing, however, it is important to note that this strictly holds true for balancing using an active ankle; this result does not reflect potential disadvantages introduced to walking provided by an arbitrarily large foot design. The heavier the system, the more torque is needed to recenter the system's mass about its unstable equilibrium point. The larger the foot, the harder it will be to keep the foot from unwanted collisions with uneven surfaces. The effect of the robot's weight can be mitigated by limiting the about the robot will rotate, effectively limiting ϕ shown in figure 6.2b, but this negatively affects the robot's range of motion, which could be undesirable.

It is also important to note the rotational speed of the motor and how it affects the system's torque. By observing Equation 6.3, it is easy to see that larger rotational speeds in general serve to decrease the applied torque. Figure 6.3 shows an exact

relation between our motor's torque output and rotational speed. This implies that to rotate the weight of the robot fluidly using an active ankle, the motor must turn as slowly, which can be an implausible solution; faster response times are generally more desired and a certain rotational bandwidth needs to be achieved to stabilize the system with an active ankle. If the motor does not rotate fast enough, the system cannot properly balance itself. This concept will be explained in more detail in the following chapter.

As important as these conclusions are in selecting a motor, these equations do not account for nonlinearities in the motor's behavior, which are prevalent for our application. Typically, a motor has to overcome nonlinearities to start running at a certain speed for these equations to be completely accurate. For robotics applications, motors instead turn back and forth, as opposed to run in a certain direction for a given amount of time, meaning there is a lot more nonlinear behavior to account for in robotics than in typical actuator applications. This does not, however, mean that these calculations do not provide insight. By analyzing and applying these relations and equations, we are able to tell the effect of increasing the height of the robot on torque, as well as increasing the foot size, and the relationship between motor speed and torque. It still remains, however, that these calculations may be insightful, but might ultimately lack the information necessary to choose the optimal motor in terms of torque requirements, and additional simulations may be needed to verify motor selection after using this criteria.

Chapter 7

SIMULATED RESULTS

To better understand how to control the system, it is not enough to simply observe the root locus. The question that needs to be addressed is what the best design for the ankle of the system would be, and whether an actuator is enough to properly control the foot. Figure 7.1 shows the frequency response of the inverted pendulum. By observing the frequency response, we can determine the appropriate controllers to try. Figure 7.1 shows a phase response of 180 degrees, meaning that a lag controller would not stabilize the system. To stabilize the system, since we need to add phase, so PD and PID controllers will be utilized. Since the current height of the system is at 0.226 meters, by using the simulation it was found that a good bandwidth for stabilization without the assistance of a passive ankle is 15 radians per second. The first two subsections do an analysis of controller performance with this stabilizing bandwidth,

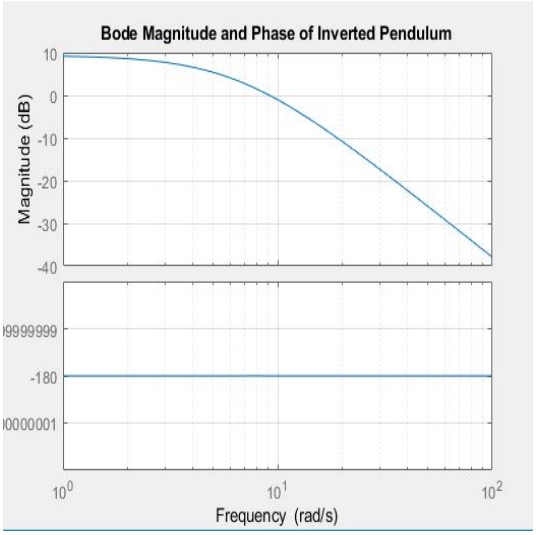

Figure 7.1: Bode of Inverted Pendulum

then the proceeding section will apply a bandwidth consistent with the rotational speed of the Dynamixel-XL430-W350-T currently installed on the leg. Using the performance graph of these motors in Figure 6.3, by observation, it can be concluded that any torque between $0.3Nm$ and $1.5Nm$ will result in a bandwidth, or RPM, of at least 40 revolutions per second, which corresponds to a bandwidth of 4.18 radians per second.

7.0.1 PD Control

The following is an analysis on PD control and whether it is the best way to control the ankle orientation, and what this can tell us about the desired design parameters of the system. To stabilize the system, the following PD controller transfer function in equation 7.1 was supplied to the system. Using the height of the robot and the analysis done in Chapter 5, a bandwidth of 15 radians per second was chosen to arrive at stable solutions an analyze the PD controller's response. The corresponding bode plot of the newly controlled system is shown in Figure 7.2.

$$PD = \frac{0.1029s + 0.4645}{0.01s + 1} \tag{7.1}$$

The following bode plot primarily shows an improved phase response where the PD controller was designed to supply the system with a phase margin of 60 degrees. A 60 degree phase margin is typical for most applications because it is a requirement for the peak sensitivity to remain below a maximum of 2 dB, but it does not necessarily guarantee a peak sensitivity of 2 dB. The peak sensitivity is directly related to disturbance rejection, where the lower the peak sensitivity (S), the better the system is at rejecting disturbances, which is very advantageous when developing a robustly stable system built primarily to overcome disturbance forces while balanced at an unstable equilibrium. The tradeoff for having a robustly stable system is described

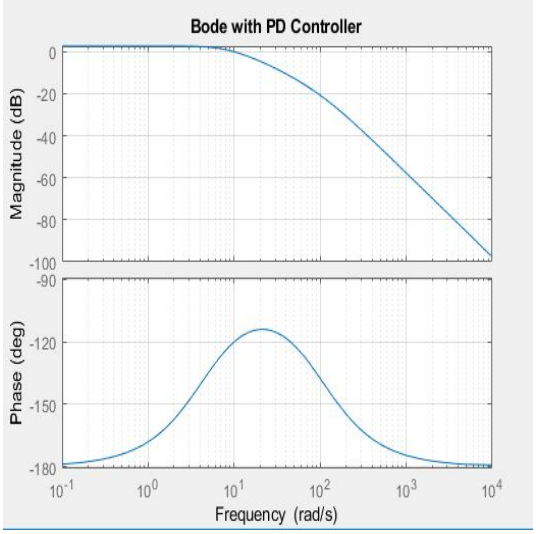

Figure 7.2: Bode of Inverted Pendulum with PD Controller

by Equation 7.2, where the term T represents complimentary sensitivity. In a well controlled system, S directly relates to disturbance rejection, while T relates to good low frequency command following and high frequency noise attenuation. For the purposes of this project, we are not as concerned with command following and high frequency noise attenuation because we are developing a balancing system tasked to reject disturbances, but the effect on T still needs to be taken into account as a very poor T can lead to limited command following and large errors due to sensor noise.

$$T + S = 1 \tag{7.2}$$

Figure 7.3a shows the sensitivity and complementary sensitivity of the system, while Figure 7.3b illustrates the step response. By observing the bode plot in Figure 7.3a it is seen that setting the phase margin to 60 degrees is not enough to produce desirable sensitivity properties, as the sensitivity is shown to be well above 0dB at low frequencies, which means it will amplify low frequency disturbances and likely produce an unstable system. The step response in Figure 7.3b shows that with a step

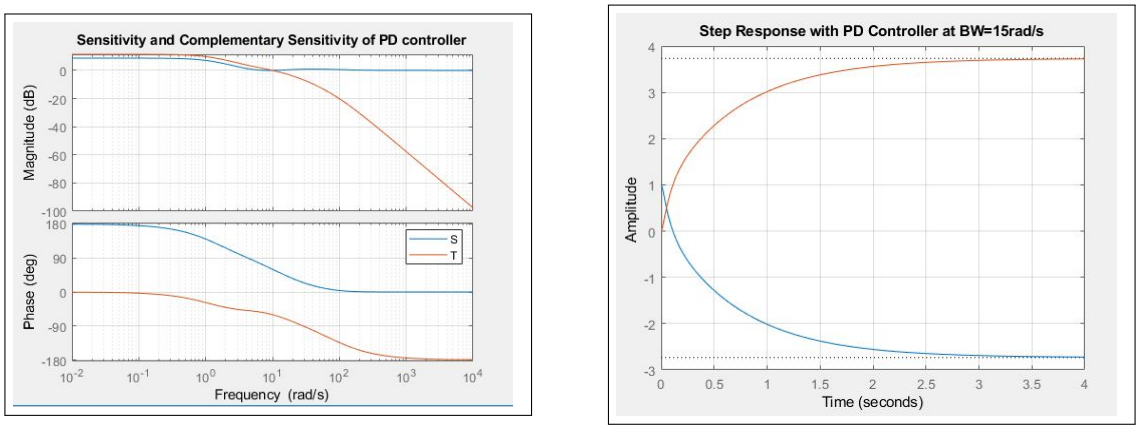

(a) (b)

Figure 7.3: T and S frequency responses of PD Controller at BW = 15rad/s (a) and step response at BW = 15rad/s (b)

input reference command, the complementary sensitivity does not return a steady state value of 1. This error between the reference signal and the output signal could cause issues when attempting to stabilize the system, so it makes sense to turn over to the PID controller to see how it compares as a good control system for the ankle.

7.0.2 PID Control

The following PID controller was designed by placing two zeros on the real axis to create phase lead, one pole far from the origin to guarantee the system's frequency response would attenuate at high frequencies and one pole at the origin as an integrator to guarantee zero steady state error. The transfer function for the PID controller developed is shown in Equation 7.3.

$$PID = \frac{0.1079s^2 + 0.4645s + 0.4998}{0.01s^s + s} \tag{7.3}$$

The PID controller produced better results. The bode plot of the inverted pen-

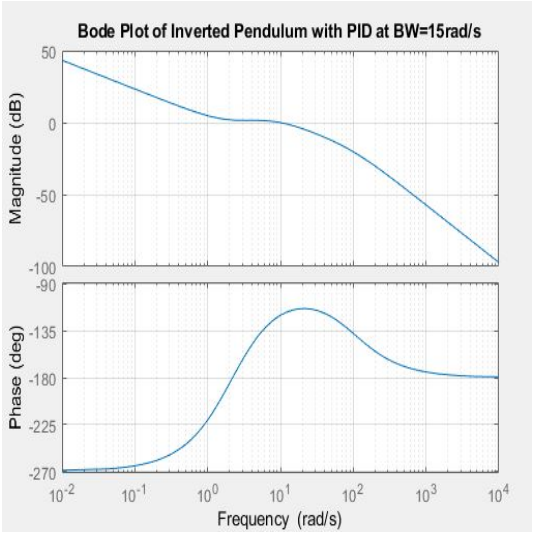

Figure 7.4: Bode of Inverted Pendulum with PID Controller

dulum with an applied PID controller can be viewed in 7.4. Similar to the PD controller, it solves for a phase margin of 60 degrees to help achieve desirable sensitivity properties, and its bode magnitude plot shows low frequency amplification for good low frequency command following, and high frequency attenuation for good high frequency noise rejection. As mentioned earlier, the sensitivity and complementary sensitivities of the system are important in determining how well the controller follows input command and rejects disturbances. Figure 7.5a shows that the general frequency response of the sensitivity and complimentary sensitivity are good, with the S attenuated at low frequencies and steady at 0dB at high frequencies, while the T is amplified at low frequencies and attenuated at high frequencies. Despite the improved performance, there is a peak in the bode plot in Figure 7.5a that corresponds to large oscillations in the step response shown in Figure 7.3b. These large oscillations are due to the low bandwidth of the system in comparison to the system's unstable pole, and the zeros near the origin placed by the PID controller. To correct this error, a prefilter W was concatenated into the reference signal to help attenuate

unwanted overshoot, resulting in an attenuated signal seen in Figure 7.5b.

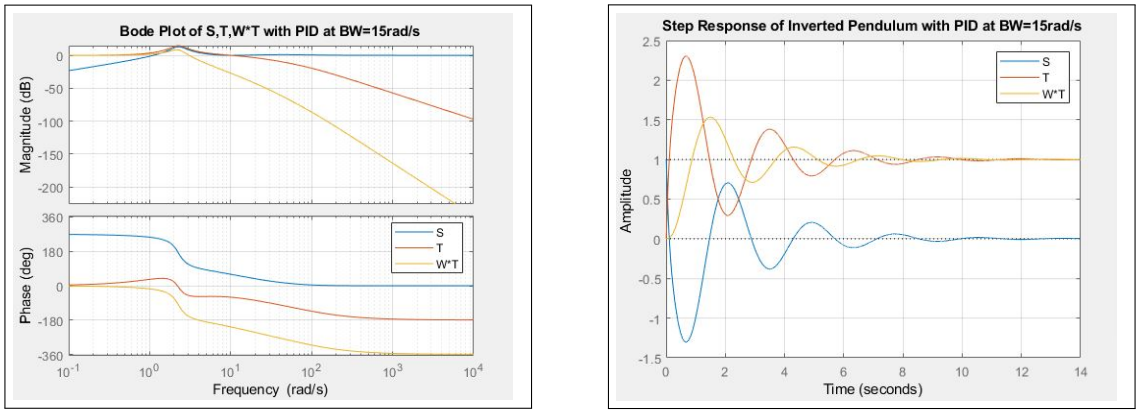

(a) (b)

Figure 7.5: T,S,W*T frequency responses of PID Controller at BW = 15rad/s (a) and step response at BW = 15rad/s (b)

These two simulations show that a PID controller makes more sense for its zero steady state error and its improved sensitivity robustness. The oscillatory behavior of the step response is still undesirable and could be attenuated further with a more complex LQR method, but instead of experimenting with different controllers, it would be more beneficial to the design process to use realistic bandwidth parameters that correspond to the motors chosen and determine if passive components can help improve design.

7.0.3 Design with the Actuator's Bandwidth

The following results illustrate the system's step response in the presence of disturbances at a bandwidth of 4.2 rad/s instead of 15 rad/s. Figure 7.6a shows a purely active ankle's step response at the motor's speed of 4.2 rad/s. Comparing the bandwidth of the system to the location of the unstable pole from Figure 5.3, it can be shown that regardless of which controller is used on the system, the result cannot

stabilize in the presence of step disturbances because the motor cannot rotate fast enough to overcome its instability. Notice that the bode plot in Figure 7.6b shows two crossovers. When the bandwidth of the system is lower than the unstable pole, it creates a second crossover in the magnitude plot that results in an instability. This change results in a change in the Nyquist encirclements of the system, which show the system to be unstable.

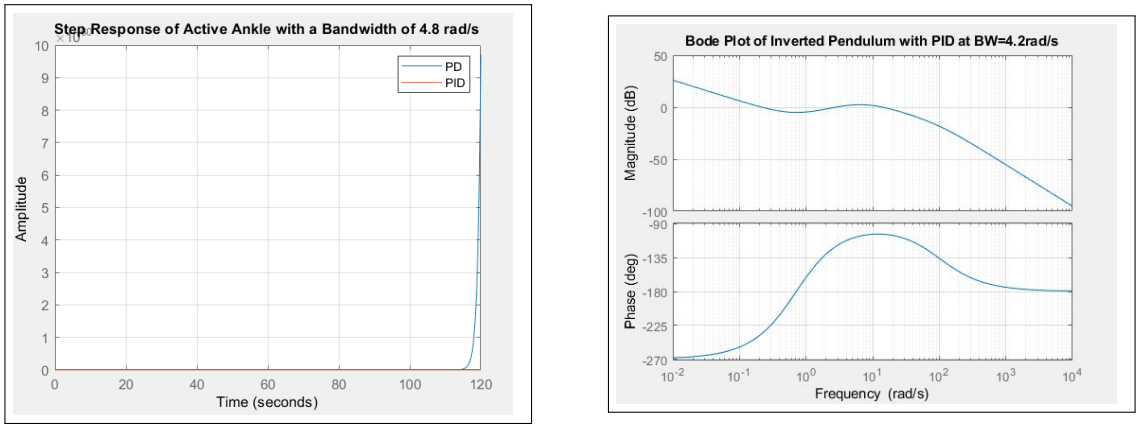

(a) (b)

Figure 7.6: Step responses of purely active ankle at 4.2 rad/s (a) and bode plot of unstable system (b)

Although this result may seem unfavorable, in Chapter 5, it was shown that the location of the right half plane pole could be dragged towards the origin by applying a torsional spring at the ankle. This spring would act as a passive controller, adding a passive proportional control to the system to help attenuate high frequency dynamics so the actuator can stabilize the system. Using the Matlab simulation, different torsional spring resistances can be applied to determine the optimal torsional spring resistance for stabilization.

The results in Figure 7.7 show the torsional spring values that result in a stable configuration for a balancing leg. Through simulation, it can be shown that depending

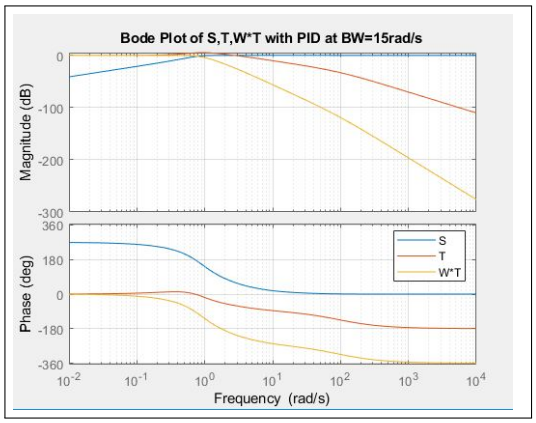

(a)

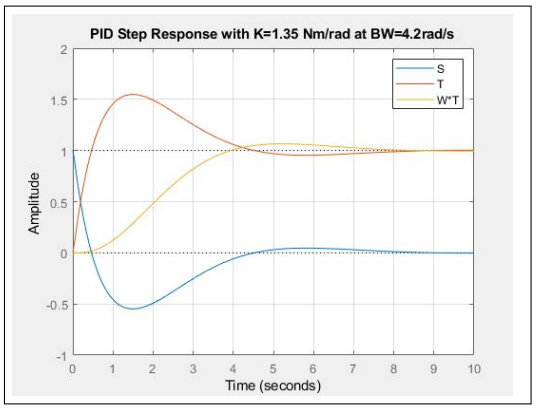

(b)

Figure 7.7: Step Response for Ankle, BW = 4.2 rad/s, K = 1.25 NM/rad (a) BW = 4.2 rad/s, K = 1.35 Nm/rad

on desired design parameters, one can tweak the desired torsional spring resistance until the optimal response is achieved. In the case of this system, the optimal response for the Dynamixel XL430-W350-T model comes from incorporating a torsional spring resistance of 1.35 rad/s. This Matlab simulation of an inverted pendulum model with a torsional spring can also be used to determine the optimal bandwidth that achieves the performance one may be looking for. By using the torsional spring resistance and bandwidth of the motors as tuning knobs, a designer can help determine not only how to best stabilize their system, but what motors and components would work best in doing so.

Lastly, due to the nature of the system, the idea of implementing LQR is intuitive due to its stability robustness properties. When implementing LQR, it guarantees that the system's peak sensitivity never exceeds 0dB. However, by observing Figure 7.7a, it is evident that when using this design, the S magnitude does not exceed 0dB when using PID, so there is no real need to implement LQR because the system's response already produces this property. It is important to note, however, that this

is due to the fact that this is a simple system with one unstable pole, and for more complex systems, it may make sense to use a more complex controller.

Chapter 8

CONCLUSION

Through experimentation, it became apparent that the quick manufacturing methods in association with laminate robotics were adequate in determining a design that could support itself, but it was insufficient in accurately providing a map for appropriate motors and link lengths necessary for high level design. Experimentation led to a shorter design that used motors designed primarily to meet the torque requirements of the system. However, upon reaching the final experimental design, it was apparent that the actuator responsible for ankle rotation could not stabilize the system fast enough without help from passive components. It was at this point the design process turned to simulation and theory to understand why and how design parameters affect motor and component selection.

Analyzing the system's dynamics revealed many tradeoffs that need to be taken into account during design. Changing the size of the leg links can affect the torque needed from each motor in various ways. By analyzing the dynamics of the system, one can determine that a taller foot requires more torque from the motors tasked with lifting the foot, because the longer the leg, the longer the double pendulum is when fully extended, so the more torque is needed for them to lift the leg in its worst case orientation. Also, the taller the leg is, the more torque is needed for the ankle actuator to rotate the leg around its foot because longer beams take more torque to rotate. However, a wider foot corresponds directly to more torque exerted by the rotational motor, because again, a longer lever arm twisting the body around the ankle generates more torsional power, and greater angular acceleration.

Changing the size of the links also affected the speed at which the motors need

to rotate to stabilize. After modeling the system as an inverted pendulum, it became apparent that the taller the robot, the lower the speed at which the actuator needed to rotate to stabilize, which in turn increased the torque the motor could provide. Through simulations in Matlab, control theory, and control design, it is possible to determine what the optimal ankle design is. In the case of this robot, using the Dynamixel XL430-W350-T motors resulted in a system with a stabilizing bandwidth of 4.2 rad/s and a torsional spring resistance of 1.35 Nm/rad. Complete specifications of this robot design can be viewed on Table 8.1.

Dynamixel Motor	Bandwidth	Torque Needed	Spring	Weight	Cost
XM430-W350-T	4.2 rad/s	0.894 Nm	1.35 Nm/rad	629 g	$689.70

Table 8.1: Final Robot Leg Specifications

It should be noted that the desired torque calculated in Table 8.1 corresponds to the torque needed to lift the double pendulum leg links in a typical orientation when the servo position angle is at 45 degrees. There is not enough data to determine the exact torque requirements considering nonlinear behavior, however taking the current leg design and placing it on a force plate to gather force readings as it rotates would solve for the rotational torque needed, and would be a good next step for the project. Also, these torque requirements for the leg only take into account the force of gravity acting on the robot as it raises and lowers itself. When the robot begins to walk, contact forces and the pressure on the motors from when it presses its leg down need to also be calculated when determining the torque of the motors.

After running simulations using Matlab, the conclusion can be drawn that the system could use motors that produced less torque and greater speed. This is in contrast with earlier experimental findings that the original motors did not have

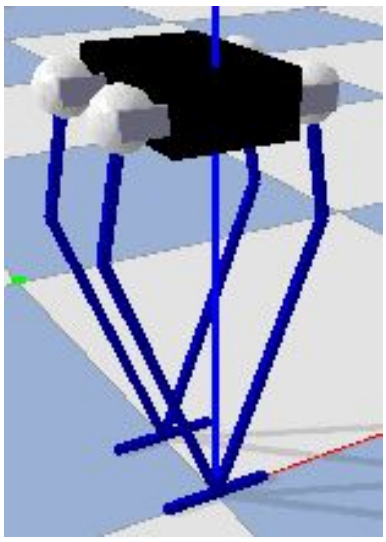

Figure 8.1: Pybullet Biped Simulation

enough torque, but by observing Table 3.1, there is a large gap in the maximum torque of both motors. Selecting a motor with stall torque specifications between $0.39Nm$ and $4.1Nm$ could prove advantageous considering the current height and design of the system, however, simulations do show that the system currently can stabilize with the correct torsional resistance, and that generally, if engineers want to develop a shorter robot, passive components will ultimately be more useful in stabilization than actuators.

8.0.1 Future Work

The end goal of this project is to design a low-cost robot that is capable of high level performance. Through experimentation, theory, and simulation, it is shown that it is possible to develop a functional leg capable of lifting its own weight, balancing, and walking, using low-cost materials. What is left is to optimize its performance for various functions. Currently, pybullet simulations are being utilized to help determine the performance of the robot.

Using physics simulations, the current design can be recreated, and by taking measurements in the lab, the simulation can be made more accurate to determine whether chosen motors will meet torque and speed requirements. These simulations, just like the theory applied to determine the torque and speed needed by the motors, rely heavily on data gathered from force plates and testing to the current system. Data gathered can paint a more clear picture about some of the nonlinearities the motors and the system experience, which can help improve simulations, and help determine optimal motors components for design.

Also, bio inspiration and material compliance were not heavily incorporated into the project so far, largely because until recently it has been in its nascent stages. As the design develops, data could be gathered on the optimal material thicknesses. Compliance can act as a spring as the robot walks, which can prove advantageous for many existing robot designs utilizing spring loaded inverted pendulum models for locomotion. Material compliance can also be simulated using physics simulations as proportional spring stiffnesses located at the physical center of each link.

Lastly, all the modeling and design choices were primarily made in two dimensions, which works well enough for balancing, however, when the robot begins walking, it will need to balance in three dimensions, meaning the robot will need to keep from tipping over as it lifts its legs. Again, further design work and simulations can be utilized to help determine a way for the robot to move in three dimensions.

REFERENCES

[1] N. C. Heglund, C. R. Taylor, F. Umana, and R. T. Mechanical, "Mechanical work basic mechanisms in terrestrial locomotion: two for minimizing energy expenditure," 2020.

[2] J. W. Grizzle, J. Hurst, B. Morris, H. Park, and K. Sreenath, "MABEL , A New Robotic Bipedal Walker and Runner," no. March 2014, 2009.

[3] S. Kuindersma et al., "Optimization-based Locomotion Planning, Estimation, and Control Design for the Atlas Humanoid Robot."

[4] J. Oh, W. Kim, J. Kim, and I. Park, "Design of Android type Humanoid Robot Albert HUBO," no. November 2006, 2014.

[5] Y. Sakagami, R. Watanabe, and C. Aoyama, "The intelligent ASIMO: System overview and integration The intelligent ASIMO: System overview and integration," no. February 2002, 2017.

[6] Q. Nguyen, A. Agrawal, W. Martin, H. Geyer, and K. Sreenath, "Dynamic bipedal locomotion over stochastic discrete terrain," 2018.

[7] M. Raibert, K. Blankespoor, G. Nelson, and R. Playter, BigDog , the Rough-Terrain Quadruped Robot, vol. 41, no. 2. IFAC, 2008.

[8] M. Fuchs, J. Zufferey, D. Floreano, and E. P. F, "A miniature 7g jumping robot," no. figure 3.

[9] H. Park, P. M. Wensing, and S. Kim, "High-speed bounding with the MIT Cheetah 2: Control design and experiments," 2017.

[10] M. Shahbazi and R. Babu, "Analytical Approximation for the Double-stance Phase of a Walking Robot," no. June, 2015.

[11] A. Singla et al., "Realizing Learned Quadruped Locomotion Behaviors through Kinematic Motion Primitives," pp. 7434–7440, 2019.

[12] A. Ramezani, J. W. Hurst, and K. A. Hamed, "Performance Analysis and Feedback Control of ATRIAS , A 3D Bipedal Robot," no. July 2015, 2013.

[13] B. A. Borovac, "Zero-Moment Point - Thirty Five Years of its Life .," no. March 2004, 2014.

[14] N. Kau, A. Schultz, N. Ferrante, and P. Slade, "Stanford Doggo: An Open-Source , Quasi-Direct-Drive Quadruped," pp. 6309–6315, 2019.

[15] S. Roberts and D. E. Koditschek, "Reactive velocity control reduces energetic cost of jumping with a virtual leg spring on simulated granular media," 2018 IEEE

Int. Conf. Robot. Biomimetics, pp. 1397–1404, 2018.

[16] A. Hereid, O. Harib, R. Hartley, Y. Gong, and J. W. Grizzle, "Rapid Trajectory Optimization Using C-FROST with Illustration on a Cassie-Series Dynamic Walking Biped," pp. 4722–4729, 2019.

[17] W. Bosworth, S. Kim, and N. Hogan, "The MIT Super Mini Cheetah: A small , low-cost quadrupedal robot for dynamic locomotion," 2015 IEEE Int. Symp. Safety, Secur. Rescue Robot., pp. 1–8.

[18] Y. Gong et al., "Feedback Control of a Cassie Bipedal Robot: Walking , Standing , and Riding a Segway," 2019 Am. Control Conf., pp. 4559–4566, 2019.

[19] Z. Xie, G. Berseth, P. Clary, and J. Hurst, "Feedback Control For Cassie With Deep Reinforcement Learning," pp. 1241–1246, 2018.

[20] J. Reher, W. Ma, and A. D. Ames, "Dynamic Walking with Compliance on a Cassie Bipedal Robot," 2019 18th Eur. Control Conf., pp. 2589–2595, 2019.

[21] D. W. Haldane, M. M. Plecnik, J. K. Yim, and R. S. Fearing, "Robotic vertical jumping agility via series-elastic power modulation," vol. 2048, no. December, 2016.

[22] E. Todorov, T. Erez, and Y. Tassa, "MuJoCo: A physics engine for model-based control," 2012 IEEE/RSJ Int. Conf. Intell. Robot. Syst., pp. 5026–5033, 2012.

[23] A. T. Baisch, O. Ozcan, B. Goldberg, D. Ithier, and R. J. Wood, "High Speed Locomotion for a Quadrupedal Microrobot," pp. 1–37, 2014.

[24] P. Birkmeyer, K. Peterson, and R. S. Fearing, "DASH: A Dynamic 16g Hexapedal Robot."

[25] A. M. Hoover, S. Burden, X. Fu, S. S. Sastry, and R. S. Fearing, "Bio-inspired design and dynamic maneuverability of a minimally actuated six-legged robot."

[26] J. W. Knaup and D. M. Aukes, "IDETC2019-98109," 2019.